### Title

Monte Carlo modeling of hepatic steatosis based on stereology and spatial distribution of fat droplets.




### Authors

Wang, Jinyang

Li, Xiaoben

Ma, Mengyuan

et al.



### Publication Date

2023-05-01

### DOI

10.1016/j.cmpb.2023.107494

Peer reviewed

HHS Public Access

Author manuscript

*Comput Methods Programs Biomed*. Author manuscript; available in PMC 2024 May 01.

Published in final edited form as:

*Comput Methods Programs Biomed*. 2023 May ; 233: 107494. doi:10.1016/j.cmpb.2023.107494.

# Monte Carlo Modeling of Hepatic Steatosis Based on Stereology and Spatial Distribution of Fat Droplets

**Jinyang Wang, PhD**[1], **Xiaoben Li**[1], **Mengyuan Ma**[1], **Changqing Wang**[1,*], **Claude B. Sirlin**[2], **Scott B. Reeder**[3,4,5,6,7], **Diego Hernando**[3,4]

[1]School of Biomedical Engineering, Anhui Medical University, Hefei, China

[2]Department of Radiology, University of California San Diego, San Diego, California, USA

[3]Department of Radiology, University of Wisconsin, Madison, Wisconsin, USA

[4]Department of Medical Physics, University of Wisconsin, Madison, Wisconsin, USA

[5]Department of Biomedical Engineering, University of Wisconsin, Madison, Wisconsin, USA

[6]Department of Medicine, University of Wisconsin, Madison, Wisconsin, USA

[7]Department of Emergency Medicine, University of Wisconsin, Madison, Wisconsin, USA

## Abstract

**Background and Objective:** To model hepatic steatosis in adult humans with non-alcoholic fatty liver disease based on stereology and spatial distribution of fat droplets from liver biopsy specimens.

**Methods:** Histological analysis was performed on 30 adult human liver biopsy specimens with varying degrees of steatosis. Morphological features of fat droplets were characterized by gamma distribution function (GDF) in both two-dimensional (2D) and three-dimensional (3D) spaces from three aspects: 1) size distribution indicating non-uniformity of fat droplets in radius; 2) nearest neighbor distance distribution indicating heterogeneous accumulation (i.e., clustering) of fat droplets; 3) regional anisotropy indicating inter-regional variability in fat fraction (FF). To generalize the morphological description of hepatic steatosis to different FFs, correlation analysis was performed among the estimated GDF parameters and FFs for all specimens. Finally, Monte Carlo modeling of hepatic steatosis was developed to simulate fat droplet distribution in tissue.

**Results:** Morphological features, including size and nearest neighbor distance in 2D and 3D spaces as well as regional anisotropy, statistically captured the distribution of fat droplets by the GDF fit ($R^2 > 0.54$). The estimated GDF parameters (i.e., scale and shape parameters) and

[*]**Corresponding author:** Changqing Wang, PhD, School of Biomedical Engineering, Anhui Medical University, Hefei (230032), China, wangchangqing@ahmu.edu.cn, Telephone: +86 0551 6516 5695.



CONFLICTS OF INTEREST

The authors declare that they have no conflict of interest.

FFs were well correlated, with $R^2 > 0.55$. In addition, simulated 3D liver morphological models demonstrated similar sections to real histological samples both visually and quantitatively.

**Conclusions:** The morphology of hepatic steatosis is well characterized by stereology and spatial distribution of fat droplets. Simulated models demonstrate similar appearances to real histological samples. Furthermore, the model may help understand MRI signal behavior in the presence of liver steatosis.

### Keywords

hepatic steatosis; simulation; fat droplet; stereology; spatial distribution

## 1. INTRODUCTION

As a manifestation of metabolic syndrome, non-alcoholic fatty liver disease (NAFLD) is commonly associated with comorbidities such as obesity, diabetes mellitus, and dyslipidemia, and it affects approximately 25% of the world's adult population (1,2). NAFLD is characterized by hepatic steatosis (i.e., excessive accumulation of triglycerides in hepatocytes), which can progress to non-alcoholic steatohepatitis, fibrosis, and even cirrhosis (3). The current reference standard for assessment of hepatic steatosis is percutaneous liver biopsy, which permits comprehensive evaluation of liver fat content as well as other key histological features in the sampled tissue.

In histological assessment of hepatic steatosis, fat droplets (i.e., cytoplasmic vacuoles) are identified as ovoid clear voids in histology slides. Hepatic steatosis severity is typically determined by visual estimation of the percentage of hepatocytes with intracellular fat droplets, and graded using an ordinal 0–3 scale (4). To reflect the actual amount of fat, fat fraction (FF) can be quantified as the volume fraction of liver parenchyma comprised by fat (5,6). The size of fat droplets, in addition to the overall quantity of fat, may be important in evaluating fatty liver disease and liver function, and there is a need to develop methods to assess fat droplet size and its statistical distribution (7). Other histological features, such as steatosis type (microvesicular, macrovesicular, or mixed) and zonality (zone 1 predominant, zone 3 predominant, azonal, or panacinar), are also relevant for fatty liver evaluation (8,9) and might benefit from quantitative analysis.

Previous work by Shrestha et al. (10) characterized fat droplet distribution with respect to two-dimensional (2D) morphological features (size, nearest neighbor distance and regional anisotropy) for 16 mouse liver samples, and developed virtual steatosis models for the calibration of MRI transverse relaxation rate (R2*) and FF. However, fat droplets show differences in size and other morphological features for human versus mice livers (11,12). In addition, the morphological droplet features were based on 2D histology slides, and may not reflect fat droplet distribution in three-dimensional (3D) liver parenchyma. Stereology, which assesses samples in 3D space, has been used for quantitative assessment of steatosis in liver biopsies, and has shown superior performance to morphometry (9,13). Description of fat droplet distribution in 3D space could serve as a model for the real histologic appearance, and help understand the relevant MRI signal behaviors (e.g., R2*-FF calibration).

Therefore, the purpose of this study was to characterize morphological features (size and nearest neighbor distance in both 2D and 3D spaces, as well as regional anisotropy) of fat droplets from human liver biopsy samples using stereology and spatial statistics. In addition, characterization of steatosis morphology was generalized to FFs in the clinically relevant range. Finally, a Monte Carlo model of hepatic steatosis was developed to model the distribution of fat droplets in 3D space. The main contributions of this work can be summarized as follows:

1. Liver biopsy specimens from adult humans with NAFLD are histologically analyzed to characterize and model hepatic steatosis.
2. The morphological features of fat droplets, including size, nearest neighbor distance and regional anisotropy, are statistically described using stereology over a clinically relevant range of FFs.
3. The model for hepatic steatosis demonstrates striking similarity with respect to real liver samples both visually and quantitatively.

## 2. MATERIALS AND METHODS

This study was performed as a secondary analysis at one site of a prospective two-center study. For the prospective two-center study, severely obese adult subjects who underwent weight loss surgery were enrolled. Potential participants with excess alcohol consumption or clinical, laboratory, or histological evidence of any liver disease other than NAFLD, and participants with contraindications to MRI (e.g., claustrophobia and metallic implants) were excluded. All subjects had intraoperative biopsy, and biopsies were scored by a pathologist using the Non-alcoholic Steatohepatitis Clinical Research Network scoring system (14). For this secondary analysis, a total of 30 subjects (6 males and 24 females, 50 ± 12 years, range 28 to 68) were selected randomly at one of the two sites, and thus all subjects either had normal livers or had NAFLD with varying degrees of steatosis. The study was approved by the local ethics committee, and all subjects gave their written informed consent.

Subjects underwent wedge biopsy from the left lobe at the time of weight loss surgery, and liver biopsy specimens were obtained. The specimens were formalin-fixed and paraffin-embedded, serially sectioned to 5 μm, mounted onto adhesive slides, and stained with hematoxylin and eosin (H&E). High-resolution digitized histology images were captured at × 40 magnification. A sufficiently large region of interest was selected from each histology image, and then processed using Image Pro Plus 6.0 software (Media Cybernetics, Inc., Rockville, MD). Preliminary segmentation of fat droplets was first achieved by the color cube based technique. Specifically, a color cube based threshold was created by selecting the pixel value within the region of interest, and was used to segment white pixels in the image. Refinement step was then employed to manually process the inaccurate segmentations, such as the mismarked, unmarked, or adherent cases. Each fat droplet was approximated as a sphere, and represented as a circle in the 2D biopsy slide. Radii and coordinates of fat droplets were then obtained, and statistical analysis was implemented using MATLAB (R2016b, MathWorks, Natick, MA). In addition, the source code and MATLAB-based

graphical user interface were shared to enable widespread dissemination of this work (https://github.com/ChangqingWangAHMU/Monte-Carlo-Modeling-of-Hepatic-Steatosis).

Morphological features of hepatic steatosis were characterized with respect to three criteria: 1) size (i.e., radius) distribution in 2D and 3D spaces; 2) nearest neighbor distance distribution in 2D and 3D spaces; 3) regional anisotropy indicating inter-regional variability in FF. As an asymmetrical distribution, the gamma distribution has wide applications and is the general form of exponential, chi-squared and Erlang distributions (15). Thus, the morphological features of hepatic steatosis were characterized by the Gamma distribution function (GDF) fit, which is formulated as:

$$GDF(x) = \frac{1}{\beta \times \Gamma(\gamma)} \times \left( \left( \frac{x}{\beta} \right)^{(\gamma - 1)} \times \exp\left( -\frac{x}{\beta} \right) \right) \quad [1]$$

where the scale parameter β and the shape parameter γ are unknown positive values, describing the width and skewness of the distribution respectively, $x$ is non-negative value denoting size or nearest neighbor distance of fat droplet (unit in micrometer), or subregional FF (unit in percentage) in the following analysis, and the gamma function $\Gamma(\gamma)$ is defined as:

$$\Gamma(\gamma) = \int_0^{\infty} x^{\gamma - 1} e^{-x} dx \quad [2]$$

## 2.1 Morphological analysis

**1) Size distribution—**For each specimen, the 2D size histogram was directly obtained from the radii of fat droplets with class interval of 1 μm. In Figure 1, the 3D size histogram was indirectly estimated by a sphere unfolding procedure based on the Scheil-Schwartz-Saltykov method (16).

Specifically, given a 2D size histogram with number of bins $m$ and relative frequency $N_A$, the corresponding frequency in 3D space ($N_v$) can be estimated by the following formula:

$$N_v(\mathrm{j}) = \sum_{i=1}^{m} \alpha_{ji} N_A(i) \quad [3]$$

where $i, j$ define the histogram bins (1, 2, 3, …, $m$), and $\alpha_{ji}$ are computed from the inverse of the matrix coefficients $k_{ji}$, which is defined as:

$$k_{ij} = \sqrt{(j^2 - (i-1)^2)} - \sqrt{(j^2 - i^2)} \quad [4]$$

**2) Nearest neighbor distance distribution—**The nearest neighbor distance is defined as the distance between centroids of a fat droplet and of its nearest fat droplet. For each specimen, the nearest neighbor distance for each fat droplet in 2D space was estimated from the coordinates of fat droplets, and the 2D nearest neighbor distance histogram was then obtained. The distribution of nearest neighbor distance for fat droplets in 3D space cannot be calculated directly, so an indirect procedure was adopted (Figure 2).

Specifically, grid coordinates were generated over reasonable ranges (0, 25] for GDF parameter β and (0, 5] for GDF parameter γ with spacing of 0.1. For each grid coordinate, a virtual 3D liver volume was simulated by incorporating the corresponding 3D size distribution, regional anisotropy, and 3D nearest neighbor distance distribution with the provided grid coordinate (see the following sections for details). A random section with thickness of 5 μm was sliced from the simulated 3D liver volume, and 2D nearest neighbor distance histogram of fat droplets in the section was fitted to the GDF. For all liver volumes generated with above grid coordinates (number of 250 × 50), the fitted GDF parameters were compared with those from the real histological section to select the optimal 3D liver model. For each specimen, the nearest neighbor distance for each fat droplet in 3D space was estimated according to the coordinates of fat droplets in the corresponding 3D liver model, and the 3D nearest neighbor distance histogram was obtained.

**3) Regional anisotropy—**Regional anisotropy was performed to characterize heterogeneity in the spatial distribution of fat droplets across different regions of the liver biopsy sample. Liver biopsy samples were gridded into 160 μm side square regions, which was approximately the size of eight hepatocytes. A random point was produced for each liver biopsy sample, and grids (or subregions) were generated along the orthogonal dimensions with step size of 160 μm. FFs for all subregions were calculated to produce the regional anisotropy histogram.

**4) Generalization of morphology description to other FFs—**To generalize the morphology description to different FFs in the clinically relevant range, regression analysis was respectively performed among FFs and the estimated GDF parameters, which were marked as $\beta_{size}$ and $\gamma_{size}$ in scenarios of size distribution in 3D space, $\beta_{nnd}$ and $\gamma_{nnd}$ in scenarios of nearest neighbor distance distribution in 3D space, $\beta_{ra}$ and $\gamma_{ra}$ in scenarios of regional anisotropy. The regression analysis was performed using OriginPro 2021 software (OriginLab, Northampton, MA), and statistical significance was accepted when $P < 0.05$. Outliers were identified by examining the absolute value of standardized residuals over a critical value according to t-distribution (17).

## 2.2 Monte Carlo modeling of hepatic steatosis

Similar to previous studies (10,18,19), a virtual 3D liver volume was simulated as cube with dimensions of 480 × 480 × 480 $\mu m^3$, consisting of 27 subcubes with dimensions of 160 × 160 × 160 $\mu m^3$. For a given overall FF in the clinically relevant range, FFs of subcubes were generated based on the regional anisotropy described above. In addition, each fat droplet was modeled as an impenetrable sphere, and spheres were determined with sizes and nearest neighbor distances following the aforementioned GDFs for each subcube. Fat droplets in each subcube were distributed one by one with a random initial sphere placement, and subsequent spheres were randomly placed with their corresponding distances in relation to target sphere. Fat droplets were placed in a nonoverlapping manner within the model: collision detection was performed after each fat droplet placed, and collision between spheres was handled by generating a new random position with the same distance. For collisions unresolved after 500 attempts, the reference sphere was regenerated to avoid a deadlock.

To evaluate the performance of the Monte Carlo modeling, simulated 2D section with thickness of 5 μm was selected from the corresponding 3D liver volume and visually compared with real histological section. In addition, their 2D morphological features were also quantitatively compared by using the Mann-Whitney $U$ test, and $P < 0.05$ was considered indicative of statistically significant difference.

## 3. RESULTS

Based on histological analysis, FFs of the 30 adult human liver biopsy specimens range from 0.5% to 24.9%. Number of fat droplets (from 257 to 5563) increases linearly with FF (unit in percentage), with a slope of 189.4 fat droplets per FF and an intercept of 423.3 fat droplets ($R^2 = 0.8626$, $P < 0.001$). Three representative samples with FFs of 3.8%, 12.3% and 24.2% are shown in Figure 3. Notice non-uniform fat droplet distribution in each case.

### 3.1 Morphological analysis

Fat droplet radii range from 2.0 to 36.5 μm. Histograms of fat droplet size as well as their GDF fits in 2D and 3D spaces are shown for the three representative liver samples in Figure 4. The distributions are well characterized by GDF fits with $R^2 > 0.79$. As FF increases, the rightward shifted histogram peak indicates an increase in the average radius of fat droplets. Compared with the GDF fits of 2D radius, higher histogram peak and identical distribution mode are observed for 3D radius of fat droplet after the sphere unfolding procedure. The histogram peak location is 6.14 ± 0.86 μm in 2D space and 6.19 ± 1.00 μm in 3D space. In addition, Figure 5 demonstrates the regression results with respect to distribution of fat droplet size in 3D space for the 30 human liver biopsy specimens. A moderate correlation is shown between scale parameter β and FF with $\beta_{size} = \exp(0.3631 \times \log(FF) + 0.6599)$ ($R^2 = 0.5499$, $P < 0.001$). Shape parameter $\gamma_{size}$ demonstrated a linear relationship with parameter $\beta_{size}$, given by $\gamma_{size} = \exp(-0.6674 \times \log(\beta_{size}) + 2.0189)$ ($R^2 = 0.9260$, $P < 0.001$). These findings suggest that fat droplet size increases as FF increases and that the morphological description of fat droplet size can be generalized to different FFs.

Nearest neighbor distance of fat droplet ranges from 6.3 to 334.2 μm. In Figure 6, histograms of nearest neighbor distance in 2D and 3D spaces are plotted for the three representative liver samples, along with their GDF fits. The histograms are well described by the GDF fits with $R^2 > 0.76$, and show similar distribution pattern. Peak locations of the histograms are relatively insensitive to FFs, while the histogram widths decrease significantly due to compact distribution of more fat droplets with increasing FF. Compared with the GDF fits of 2D nearest neighbor distance, narrow distributions along with left-shifted peaks are demonstrated in 3D space (Fig.6B). The histogram peak location is 22.45 ± 2.65 μm in 2D space and 15.38 ± 2.02 μm in 3D space. Additionally, Figure 7 provides the regression results with respect to distribution of nearest neighbor distance in 3D space for the 30 human liver biopsy specimens. Correlations among GDF parameters ($\beta_{nnd}$ and $\gamma_{nnd}$) and FF are given by $\beta_{nnd} = \exp(-0.2172 \times \log(FF) - 0.5203)$ ($R^2 = 0.5910$, $P < 0.001$, Fig.7A) and $\gamma_{nnd} = \exp(-0.6061 \times \log(\beta_{nnd}) + 2.7762)$ ($R^2 = 0.8096$, $P < 0.001$, Fig.7B). These findings indicate that fat droplet distribution becomes more crowded as FF increases

and that the morphological description of nearest neighbor distance can be generalized to different FFs.

Figure 8 shows histograms of regional anisotropy for the three representative liver samples along with their corresponding GDF fits ($R^2 > 0.54$). For the specimen with low FF, most of the subregions have no or few detectable fat droplets, and account for a large proportion in the histogram. For increasing FFs, the right-shifted histogram peaks indicate increased subregions with more fat droplets. Figure 9 shows the regression results with respect to regional anisotropy, and correlations are given by $\beta_{ra} = \exp(0.5119 \times \log(FF) + 3.2968)$ ($R^2 = 0.7040$, $P < 0.001$, Fig.9A) and $\gamma_{ra} = \exp(0.3305 \times \log(FF) + 0.8593)$ ($R^2 = 0.7571$, $P < 0.001$, Fig.9B). These findings indicate that regional anisotropy increases as FF increases and that the morphological description of regional anisotropy can be generalized to different FFs.

The morphological description of hepatic steatosis in 3D space is summarized in Table 1. By incorporating the morphological features (i.e., size, nearest neighbor distance and regional anisotropy), the Monte Carlo modeling of hepatic steatosis can be generalized to different FFs.

### 3.2 Monte Carlo modeling of hepatic steatosis

For the three representative FFs (3.8%, 12.3% and 24.2%), Figure 10 shows the simulated 3D liver morphological models, and their 2D sections (thickness of 5 μm) as well as real 2D histological sections. In scenarios of same FF, a close qualitative resemblance is observed between the simulated 2D section and real histological section. In addition, quantitative comparison of 2D morphological features also demonstrates a similar distribution of fat droplets between Figures 10D–I and 10J–O with $P > 0.085$.

## 4. DISCUSSION

In this work, we have characterized the morphological features of fat droplets for adult humans with NAFLD from liver biopsy specimens with various degrees of steatosis, including size, nearest neighbor distance and regional anisotropy. The features are well characterized by GDF fits, and morphology descriptions indicate increase trends of fat droplet size and regional anisotropy, while decrease trend of nearest neighbor distance, as FF increases. Furthermore, this study develops a corresponding Monte Carlo model of hepatic steatosis, and the model demonstrates a close resemblance with respect to real liver samples. These results may be helpful for the understanding of relevant MRI signal behaviors, as discussed further below, including the positive correlation between proton density fat fraction (PDFF) and R2* (10,20) and the negative correlation between PDFF and apparent diffusion coefficient (21).

Hepatic steatosis can be classified as microvesicular or macrovesicular steatosis according to fat droplet size, which also plays an important role in evaluating fatty liver disease (11,22,23). The severity of fatty liver disease may be associated with fat droplet size rather than the significant changes in the quantity of liver fat (7,24). As observed visually in H&E stained sections, fat droplets are demonstrated to distribute with non-constant size

and in non-uniform pattern. It should be noted that fat droplets in human liver demonstrate similar mean size but higher median size than those in mouse liver (11), where more fat is contributed by small fat droplets. In accordance with previous studies (10,25,26), distribution of fat droplet size in 2D space was well characterized by the GDF fit. In addition, different GDF parameters were demonstrated quantitatively for human liver biopsy specimens with various degrees of steatosis, and correlation was founded with FF. Though 3D data were not available, the sphere unfolding procedure was performed to obtain the 3D size histogram, which may helpful for discrimination of steatosis type (microvesicular or macrovesicular).

Spatial distribution of fat droplets in 3D space is challenging to capture due to lack of 3D data, and 2D biopsy section cannot reveal the actual distribution of fat droplets in 3D space. This study used nearest neighbor distance and regional anisotropy to characterize the clustering accumulation of fat droplets and inter-regional variability in FF. By comparing the GDF parameters of random sections and real histological samples to select the optimal 3D liver volume, the distribution of nearest neighbor distance in 3D space was obtained based on the optimal model. To analyze the inter-regional variability in FF, subregions with side length of 160 μm were used considering the size of fat droplets (maximum value is 36.5 μm) as well as hepatocyte (approximately 20 μm). These two features were well characterized by the GDF fits, which agree well with a previous study for mice liver histology images (10).

In contrast to previous simulations based on morphological features of fat droplets from 2D biopsy sections (10,25), this study characterized the features in 3D space and developed a corresponding Monte Carlo model. Distributions of fat droplet size and nearest neighbor distance were significantly different for fat droplets in 2D and 3D spaces (Fig.4 and Fig.6). It was deemed necessary to evaluate the 3D morphological features of fat droplets from 2D tissue slices. Through statistical processing, fat droplets in the 2D virtual section showed similar distribution pattern with respect to real tissue slices.

Organization of fat deposits in tissue microstructure may be relevant to microscopic susceptibility effects, and induce relevant MRI signal behaviors (20,21,27). As an example, chemical shift-encoded MRI has been increasingly used to evaluate hepatic steatosis in clinical practices. This technique measures PDFF (unit in percentage) and R2* (unit in $s^{-1}$), which are promising biomarkers for triglyceride concentration and iron concentration, respectively (28,29). Several studies have demonstrated positive correlations of PDFF and R2* for livers without iron overload, suggesting that fat droplets cause susceptibility effects (10,20,27). Other studies have shown that steatosis is associated with restricted water diffusion, plausibly because fat droplets reduce the space available for water motion (30). An accurate morphological description of hepatic steatosis in 3D space might allow modeling of the inhomogeneous microscopic magnetic field distributions induced by fat droplets to understand MRI signal behavior in the presence of liver steatosis (10,31), such as the impact on transverse relaxation rate. Similar models could be developed to better understand the restriction of water diffusion.

This study has several limitations. First, liver biopsy suffers from sampling variability due to inhomogeneous spatial distribution of fat droplets, which is inherent feature for hepatic

steatosis (32,33), and microvesicular fat may be difficult to resolve in H&E sections viewed under the microscope (11). Second, an indirect approach was adopted to obtain the size distribution and nearest neighbor distance distribution of fat droplets in 3D space, 3D construction from a series of biopsy slides is theoretically feasible, however, a tedious and challenging process limited by the number and thickness of tissue sections. Third, a simple cubic model was used for simulation by incorporating morphological features of fat droplets, and spatial distribution of fat droplets with respect to the anatomical structures (e.g., central vein and portal tract) in whole biopsy images is also warranted in a future study (25,26). Lastly, hepatic steatosis is commonly accompanied by other histological features such as inflammation, ballooning, fibrosis and steatohepatitis. Future studies are needed to examine how these other features might affect the morphological features of fat droplets.

## 5. CONCLUSION

In conclusion, Monte Carlo modeling of hepatic steatosis was developed based on the morphological features of fat droplets for human liver biopsy samples, and the simulated 3D model demonstrated high similarity to real tissue samples. Accurate information about distribution of fat droplets in tissue microstructure may be helpful for understanding complicated MR signal behaviors. Moreover, the proposed method can also be applicable to other intracellular particles such as hemosiderin deposition, inclusion bodies or secretory vesicles.

## ACKNOWLEDGEMENTS

This work receives support from the National Natural Science Foundation of China (62001005), the Anhui Provincial Natural Science Foundation (2008085QH425), the Grants for Scientific Research of BSKY (XJ201811) from Anhui Medical University, as well as the NIH (R01 DK083380, R01 DK088925, R01 DK100651 and K24 DK102595). The authors also wish to acknowledge support from GE Healthcare who provides research support to UW-Madison. Further, Dr. Reeder is a Romnes Faculty Fellow, and has received an award provided by the University of Wisconsin-Madison Office of the Vice Chancellor for Research and Graduate Education with funding from the Wisconsin Alumni Research Foundation.

## Abbreviations:

| | |
|---|---|
| **2D** | two-dimensional |
| **3D** | three-dimensional |
| **FF** | fat fraction |
| **GDF** | gamma distribution function |
| **NAFLD** | non-alcoholic fatty liver disease |
| **PDFF** | proton density fat fraction |

## REFERENCES

1. Younossi ZM, Koenig AB, Abdelatif D, Fazel Y, Henry L, Wymer M. Global epidemiology of nonalcoholic fatty liver disease-Meta-analytic assessment of prevalence, incidence, and outcomes. Hepatology 2016;64(1):73–84. [PubMed: 26707365]

2. Szczepaniak LS, Nurenberg P, Leonard D, Browning JD, Reingold JS, Grundy S, Hobbs HH, Dobbins RL. Magnetic resonance spectroscopy to measure hepatic triglyceride content: prevalence of hepatic steatosis in the general population. Am J Physiol Endocrinol Metab 2005;288(2):E462–468. [PubMed: 15339742]
3. Chalasani N, Younossi Z, Lavine JE, Charlton M, Cusi K, Rinella M, Harrison SA, Brunt EM, Sanyal AJ. The diagnosis and management of nonalcoholic fatty liver disease: practice guidance from the american association for the study of liver diseases. Hepatology 2018;67(1):328–357. [PubMed: 28714183]
4. Brunt EM, Janney CG, Di Bisceglie AM, Neuschwander-Tetri BA, Bacon BR. Nonalcoholic steatohepatitis: a proposal for grading and staging the histological lesions. Am J Gastroenterol 1999;94(9):2467–2474. [PubMed: 10484010]
5. Kage M, Aishima S, Kusano H, Yano H. Histopathological findings of nonalcoholic fatty liver disease and nonalcoholic steatohepatitis. J Med Ultrason 2020;47(4):549–554.
6. Kondo R, Kusano H, Mihara Y, Kage M, Akiba J, Yano H. Pathological findings of liver steatosis that is difficult to evaluate with ultrasound. J Med Ultrason 2021;48(4):515–522.
7. Zhou Z, Fang J, Cristea A, Lin YH, Tsai YW, Wan YL, Yeow KM, Ho MC, Tsui PH. Value of homodyned K distribution in ultrasound parametric imaging of hepatic steatosis: An animal study. Ultrasonics 2020;101:106001. [PubMed: 31505328]
8. Carter-Kent C, Brunt EM, Yerian LM, et al. Relations of steatosis type, grade, and zonality to histological features in pediatric nonalcoholic fatty liver disease. J Pediatr Gastroenterol Nutr 2011;52(2):190–197. [PubMed: 21240012]
9. Zaitoun AM, Mardini HA, Awad S, Ukabam S, Record CO. Quantitative assessment of fibrosis and steatosis in liver biopsies from patients with chronic hepatitis C. J Clin Pathol 2001;54(6):461–465. [PubMed: 11376020]
10. Shrestha U, van der Merwe M, Kumar N, Jacobs E, Satapathy SK, Morin C, Tipirneni-Sajja A. Morphological characterization of hepatic steatosis and Monte Carlo modeling of MRI signal for accurate quantification of fat fraction and relaxivity. NMR Biomed 2021;34(6):e4489. [PubMed: 33586261]
11. Levene AP, Kudo H, Armstrong MJ, Kudo H, Armstrong MJ, Thursz MR, Gedroyc WM, Anstee QM, Goldin RD. Quantifying hepatic steatosis–more than meets the eye. Histopathology 2012; 60(6):971–981. [PubMed: 22372668]
12. Singer P, Gnauck G, Honigmann G, Honigmann G, Stolz P, Schliack V, Kettler L. The fatty acid pattern of adipose tissue and liver triglycerides according to fat droplet size in liver parenchymal cells of diabetic subjects. Diabetologia 1974;10(5):455–458. [PubMed: 4375642]
13. Zaitoun A, Al Mardini H, Record C. Quantitative assessment of fibrosis in liver biopsies from patients with alcoholic and non-alcoholic liver disease. J Clin Pathol 1999;4:11–20.
14. Kleiner DE, Brunt EM, Van Natta M, et al. Design and validation of a histological scoring system for nonalcoholic fatty liver disease. Hepatology 2005;41(6):1313–1321. [PubMed: 15915461]
15. Krakowski M The relevation transform and a generalization of the gamma distribution function. Revue française d'automatique, informatique, recherche opérationnelle Recherche opérationnelle 1973;7(V2):107–120.
16. Stoyan D, Kendall WS, Chiu SN, Mecke J. Stochastic geometry and its applications. New York: John Wiley & Sons;2013;430–432.
17. Pankratz A Forecasting with dynamic regression models. New York: John Wiley & Sons;1991;290–314.
18. Ghugre NR, Gonzalez-Gomez I, Shimada H, Coates TD, Wood JC. Quantitative analysis and modelling of hepatic iron stores using stereology and spatial statistics. J Microsc 2010;238(3):265–274. [PubMed: 20579264]
19. Ghugre NR, Wood JC. Relaxivity-iron calibration in hepatic iron overload: probing underlying biophysical mechanisms using a Monte Carlo model. Magn Reson Med 2011;65(3):837–847. [PubMed: 21337413]
20. Hernando D, Haufe WM, Hooker CA, Schlein A, Wolfson T, Artz NS, Reeder SB, Sirlin CB. Relationship between liver proton density fat fraction and R2* in the absence of iron overload. In Proceedings of the 23rd Annual Meeting of ISMRM 2015; Toronto, Canada. p. 4118.

21. Hansmann J, Hernando D, Reeder SB. Fat confounds the observed apparent diffusion coefficient in patients with hepatic steatosis. Magn Reson Med 2013;69(2):545–552. [PubMed: 23161434]
22. Neil DAH, Minervini M, Smith ML, Hubscher SG, Brunt EM, Demetris AJ. Banff consensus recommendations for steatosis assessment in donor livers. Hepatology 2022;75(4):1014–1025. [PubMed: 34676901]
23. Wang L, Yu S, Chan W. Pathology of non-alcoholic fatty liver disease. International Journal of Digestive Diseases 2016;2(1):1–14.
24. Masterton G, Ngoh LYC, Lockman A, Hayes PC, Plevris J. The significance of fat droplet size and the prognostic value of hyaluronic acid in non-alcoholic fatty liver disease (NAFLD): a biopsy based analysis. Gut 2011;60(1):A239–A240.
25. Ratliff BA, Hernando D, Wiens C, Wang C, Watson R, Agni R, Sirlin CB, Reeder SB. Liver biopsy analysis to determine fat droplet distribution. In Proceedings of the 25th Annual Meeting of ISMRM 2017; Hawaii, United States. p. 1467.
26. Batool N. Detection and spatial analysis of hepatic steatosis in histopathology images using sparse linear models. Paper presented at: 2016 Sixth International Conference on Image Processing Theory, Tools and Applications 2016; Qulu, p. 1–6.
27. Karlsson M, Ekstedt M, Dahlstrom N, Forsgren MF, Ignatova S, Noren B, Dahlqvist Leinhard O, Kechagias S, Lundberg P. Liver R2* is affected by both iron and fat: A dual biopsy-validated study of chronic liver diseasez. J Magn Reson Imaging 2019;50(1):325–333. [PubMed: 30637926]
28. Roberts NT, Hernando D, Holmes JH, Wiens CN, Reeder SB. Noise properties of proton density fat fraction estimated using chemical shift-encoded MRI. Magn Reson Med 2018;80(2):685–695. [PubMed: 29322549]
29. Colgan TJ, Van Pay AJ, Sharma SD, Mao L, Reeder SB. Diurnal variation of proton density fat fraction in the liver using quantitative chemical shift encoded MRI. J Magn Reson Imaging 2020;51(2):407–414. [PubMed: 31168893]
30. Joo I, Lee JM, Yoon JH, Jang JJ, Han JK, Choi BI. Nonalcoholic fatty liver disease: intravoxel incoherent motion diffusion-weighted MR imaging-an experimental study in a rabbit model, Radiology 2014;270(1);131–40. [PubMed: 24091358]
31. Wang J, Wang C, Reeder SB, Hernando D. Morphological Characterization of Hepatic Steatosis Using Stereology and Spatial Statistics. In proceedings of the 31rd Annual Meeting of ISMRM 2022; London, UK. p. 3802.
32. Ratziu V, Charlotte F, Heurtier A, Gombert S, Giral P, Bruckert E, Grimaldi A, Capron F, Poynard T, Group LS. Sampling variability of liver biopsy in nonalcoholic fatty liver disease. Gastroenterology 2005;128(7):1898–1906. [PubMed: 15940625]
33. Reeder SB, Sirlin CB. Quantification of liver fat with magnetic resonance imaging. Magn Reson Imaging Clin N Am 2010;18(3):337–357, ix. [PubMed: 21094444]

## Highlights

- Organization of fat deposits may affect the evaluation of hepatic steatosis.
- Hepatic steatosis is modeled according to spatial distribution of fat droplets.
- The model demonstrates striking similarity with respect to real liver samples.
- The model can help understand MRI signal behaviors for human liver steatosis.

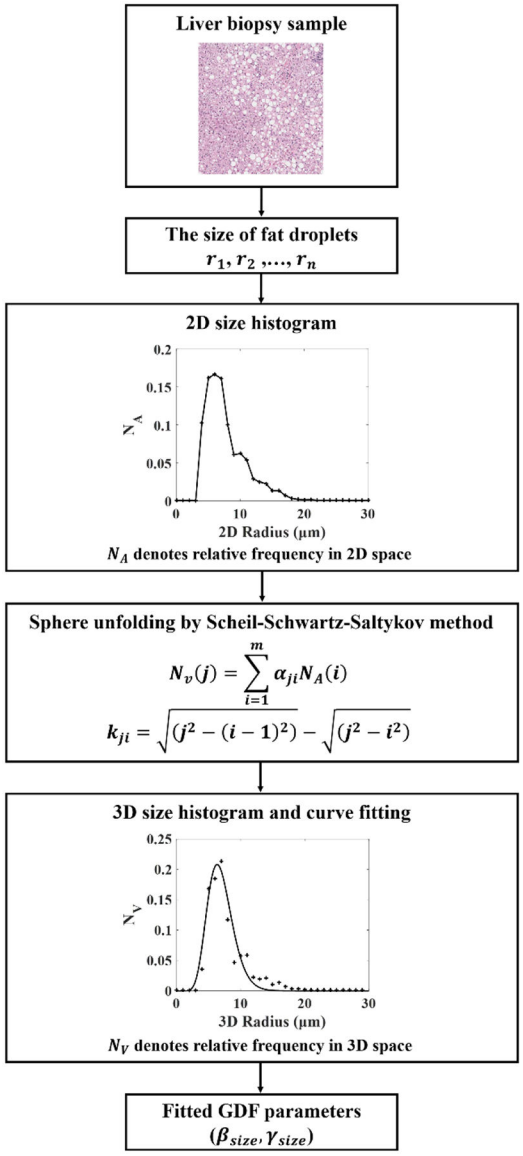


**Figure 1.**
Flowchart depicting the distribution of fat droplet size in 3D space from 2D slide.

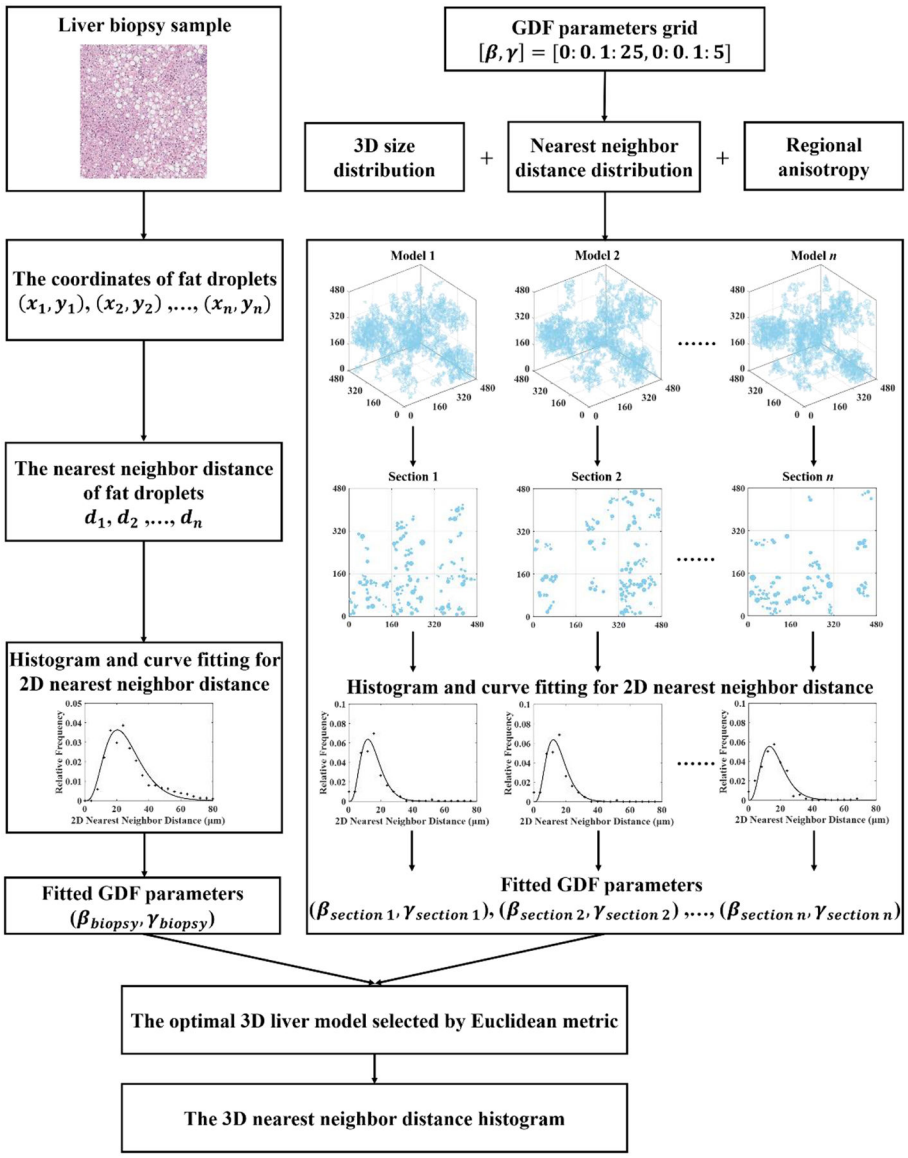


**Figure 2.**

Flowchart depicting the distribution of fat droplet nearest neighbor distance in 3D space from 2D slide.

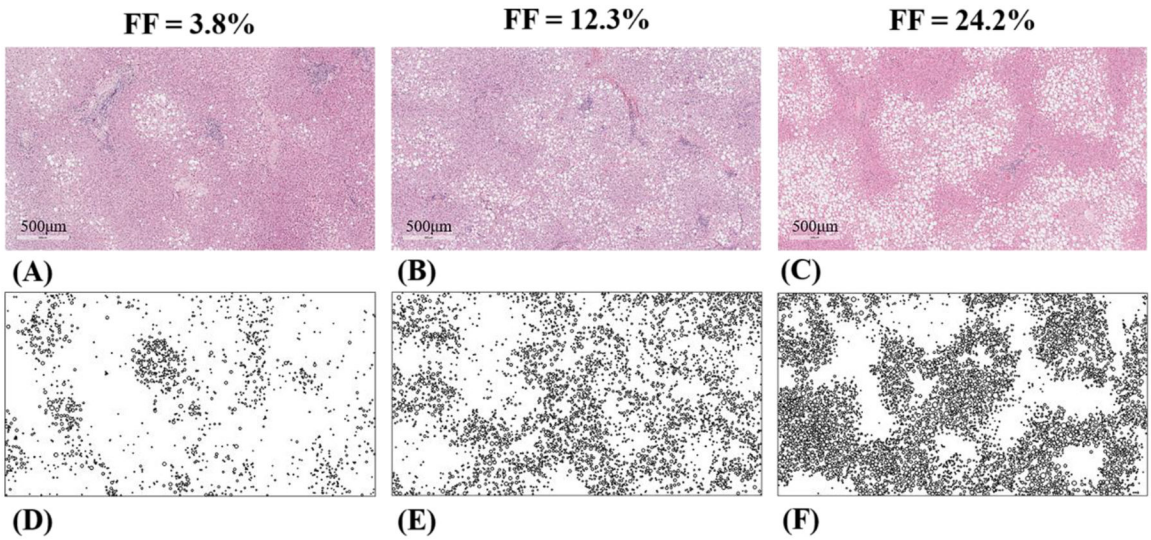


**Figure 3.**

Three representative liver biopsy samples **(A-C)** and their approximation images after morphological processing **(D-F)**. Each fat droplet, which can be approximated as sphere, is represented as a circle in 2D tissue space.

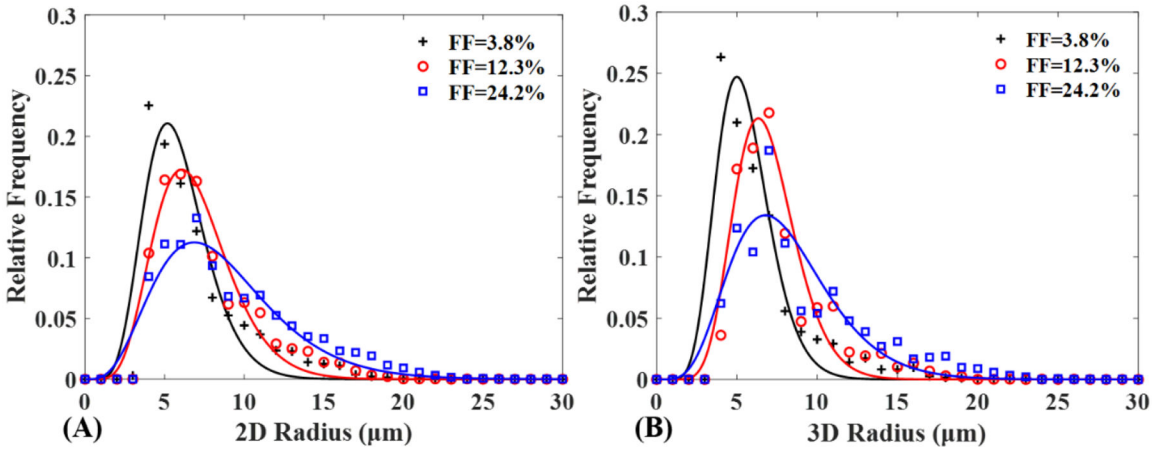


**Figure 4.**

Distribution of fat droplet size in 2D **(A)** and 3D **(B)** tissue spaces for the three representative liver biopsy samples.

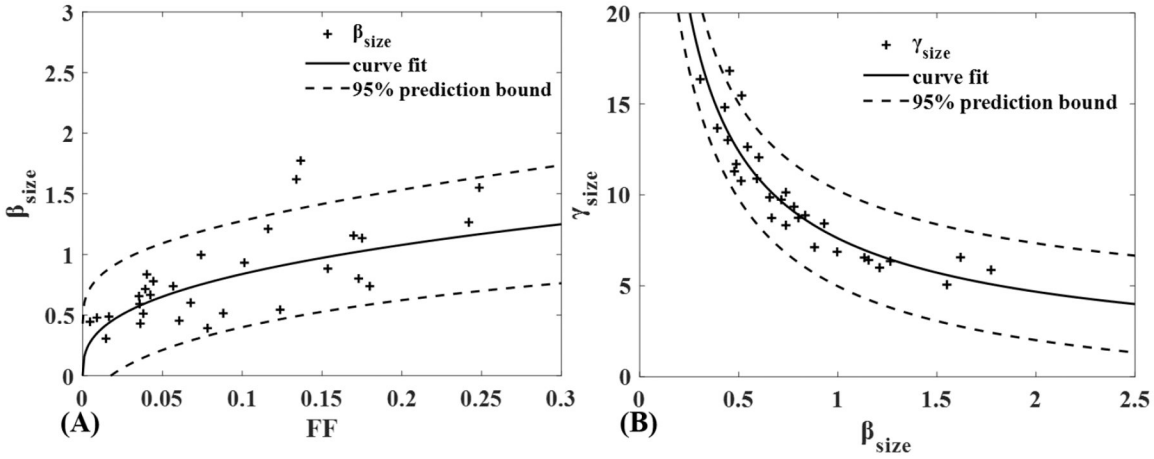


**Figure 5.**

Correlations among GDF parameters and FF for distribution of fat droplet size. **(A)** The estimated parameters $\beta_{size}$ for 30 human liver biopsy samples are plotted against FF along with curve fit. **(B)** Correlation between parameter $\beta_{size}$ and its respective parameter $\gamma_{size}$. Note that the parameters $\beta_{size}$ and $\gamma_{size}$ represent the width and skewness of size distribution, respectively.

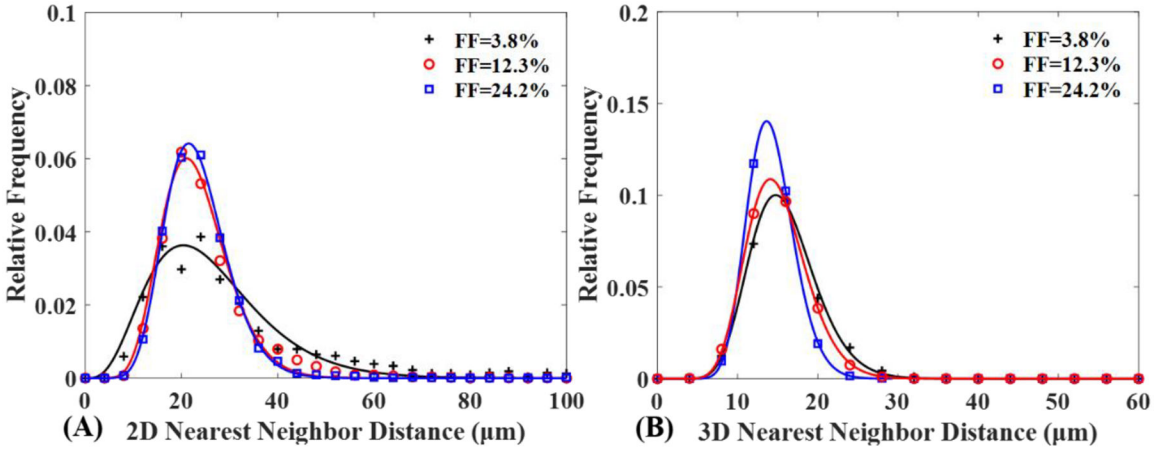


**Figure 6.**

Distribution of fat droplet nearest neighbor distance in 2D **(A)** and 3D **(B)** spaces for the three representative liver biopsy samples.

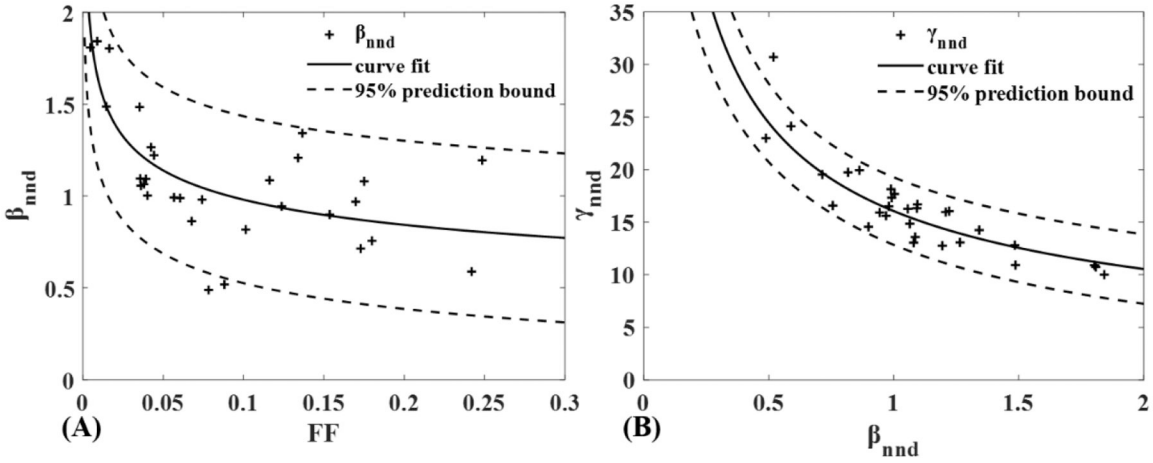


**Figure 7.**

Correlations among GDF parameters and FF for distribution of nearest neighbor distance. **(A)** The estimated parameters $\beta_{nnd}$ for 30 human liver biopsy samples are plotted against respective FF along with curve fit. **(B)** Correlation between parameter $\beta_{nnd}$ and its respective parameter $\gamma_{nnd}$. Note that the parameters $\beta_{nnd}$ and $\gamma_{nnd}$ represent the width and skewness of the nearest neighbor distance distribution, respectively.

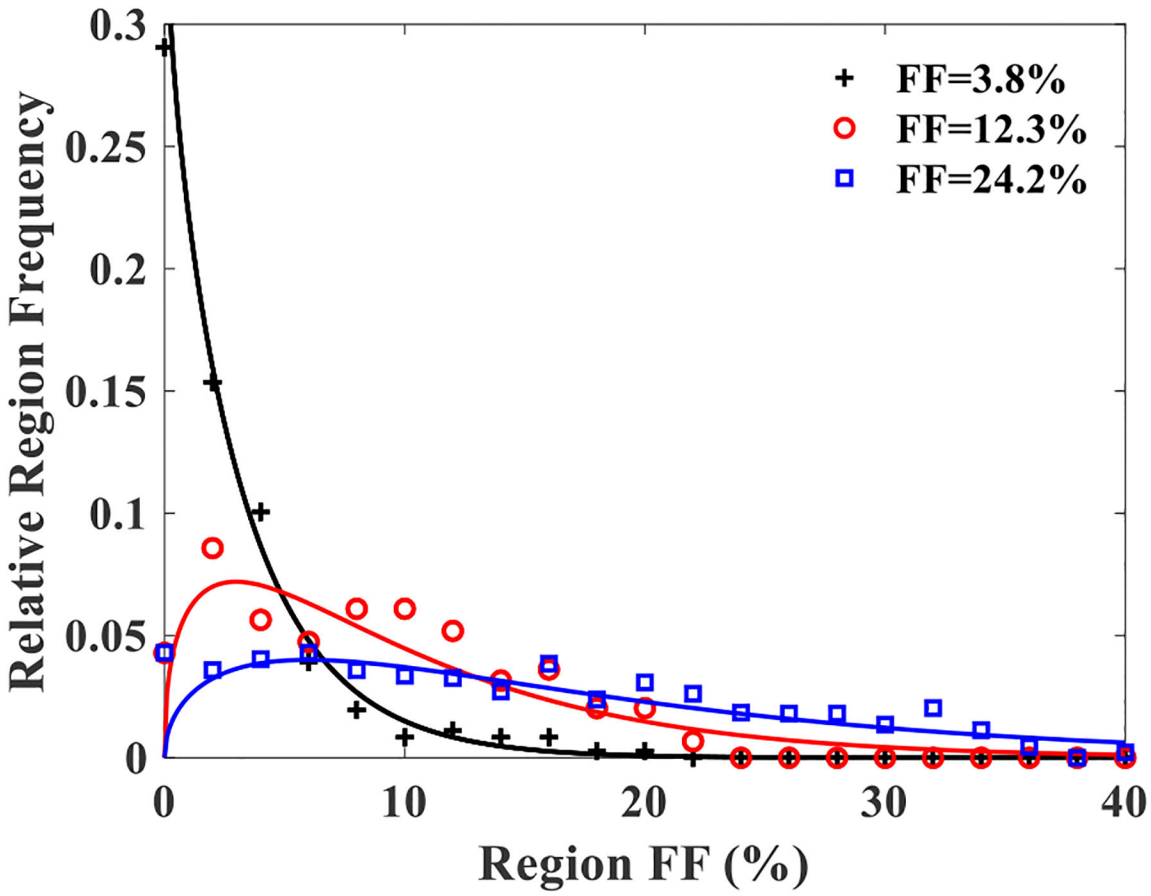


**Figure 8.**

Regional anisotropy of fat droplet for the three representative liver biopsy samples. Each liver biopsy sample was gridded into 160 μm side square subregions, approximately 64 hepatocytes, to investigate the inter-regional variability of FF. Horizontal and vertical axes shows the subregional FFs and their relative frequencies. The plots indicate the non-uniform distribution of fat droplets across regions.

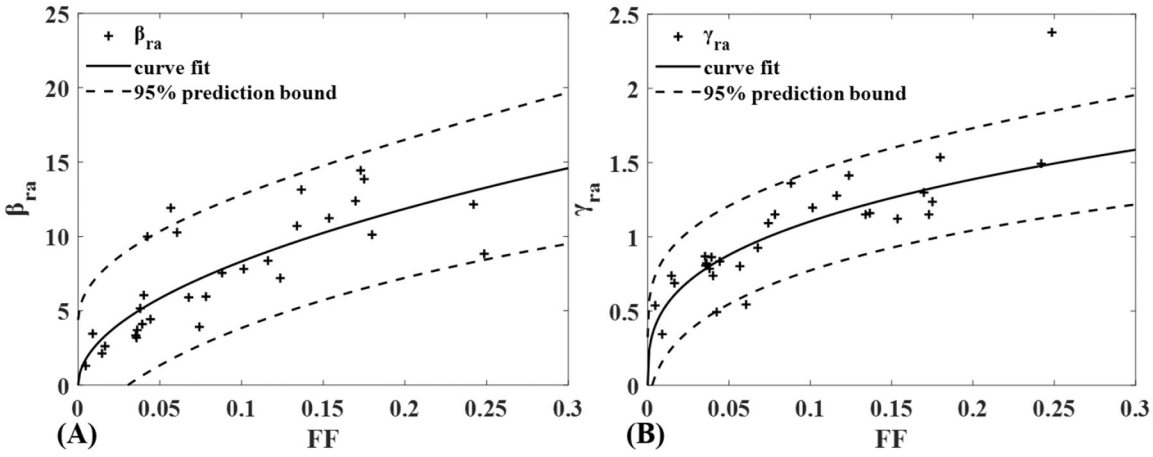


**Figure 9.**

Correlations between GDF parameters and FF for regional anisotropy. **(A)** The estimated parameters $\beta_{ra}$ for 30 human liver biopsy samples are plotted against respective FF along with curve fit. **(B)** The estimated parameters $\gamma_{ra}$ are plotted against respective FF along with curve fit. Note that the parameters $\beta_{ra}$ and $\gamma_{ra}$ represent the width and skewness of regional anisotropy, respectively.

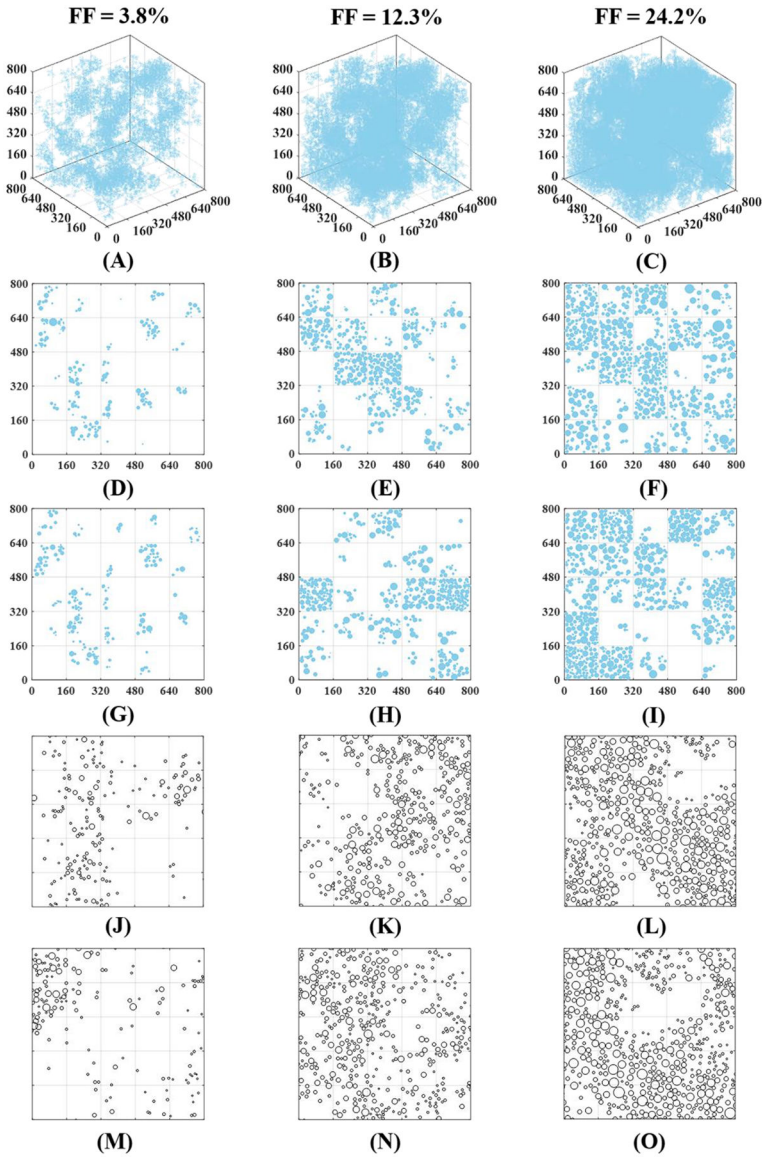


**Figure 10.**

Simulated liver fat morphology for FFs of 3.8%, 12.3% and 24.2%. **(A-C)** Simulated 3D liver morphological models with a side length of 800 μm. **(D-I)** Simulated 2D sections with thickness of 5 μm from the corresponding 3D models, solid circles represent fat droplets of different sizes. **(J-O)** Real 2D histological sections extracted from corresponding samples in Figure 3.

**Table 1.**

Morphological description of hepatic steatosis.

| Characterization | Equation | m | b | $R^2$ |
|---|---|---|---|---|
| **Size** | $\beta_{size} = \exp(m \times \log(FF) + b)$ | 0.3631 | 0.6599 | 0.5499 |
| | $\gamma_{size} = \exp(m \times \log(\beta_{size}) + b)$ | −0.6674 | 2.0189 | 0.9260 |
| **Nearest neighbor distance** | $\beta_{nnd} = \exp(m \times \log(FF) + b)$ | −0.2172 | −0.5203 | 0.5910 |
| | $\gamma_{nnd} = \exp(m \times \log(\beta_{nnd}) + b)$ | −0.6061 | 2.7762 | 0.8069 |
| **Regional anisotropy** | $\beta_{ra} = \exp(m \times \log(FF) + b)$ | 0.5119 | 3.2968 | 0.7040 |
| | $\gamma_{ra} = \exp(m \times \log(FF) + b)$ | 0.3305 | 0.8593 | 0.7571 |